ORIGINAL PAPER

Tomáš Grygar

Phenomenological kinetics of irreversible electrochemical dissolution of metal-oxide microparticles

Abstract The electrochemical dissolution of metal oxides and other stable solid phases composed of nano- to micro-crystalline particles is generally a complex process. It can be simplified by distinguishing two main contributions to the reactivity of the solid: the potential-dependent rate coefficient $k(E)$, and the conversion-dependent function $f(y)$. These contributions can be evaluated by a combination of potentiostatic and potentiodynamic experiments. Both $k(E)$ and $f(y)$ were obtained experimentally for the dissolution of iron and chromium oxides, and theoretical consequences of their particular forms are discussed. A peak-shaped function $k(E)$ was observed in the case of γ-Fe_2O_3, whereas, for α-Cr_2O_3 and CrO_2, a different model based on intermediate surface complexes is proposed. This model also explains the complete electrochemical dissolution of metal oxides regardless of their low intrinsic electric conductivity.

Key words Electrochemical dissolution · Heterogeneous kinetics · Iron oxides · Chromium oxides

Introduction

There is a remarkable variety of electrochemical reactions of transition metal oxides, such as reversible redox reactions coupled with ion insertion (W and V bronzes), solid-to-solid transformations of particles where either reactants or products are conducting (Ag, Cu, and Pb simple and mixed oxides), and redox dissolution of Fe and Cr oxides (see [1–3] for a review). The structures of the majority of Fe and Cr^{III} oxides do not contain channels for ion insertion; the oxides are chemically rather inert, and their chemical dissolution proceeds via

slow surface reactions with dissolved chemical agents (H^+, OH^-, ligands), i.e. they proceed only on the surface exposed to the solution. Among numerous dissolution reactions of metal oxides, reductive dissolution of Fe^{III} oxides and oxidative dissolution of Cr^{III} oxides have been intensively studied because they are much faster than purely ligand- or proton-promoted dissolution but usually much slower than diffusion [4]. The charge transfer can hence be a measure of their overall dissolution, which is suitable for use in electrochemical experimental methods.

Abrasive stripping voltammetry (AbrSV [1, 2]) allows direct electrochemical reactions of microcrystalline solids to be carried out. The method is not limited to conducting solids, because even non-conducting crystals can react on the ternary interface solid-electrode-solution [1, 2, 5]. However, the importance of the solid-phase conductivity and other physical properties for AbrSV is to be found in each particular electrochemical reaction. Formal reaction kinetics could be useful to process and evaluate experimental data. Recently, a theoretical description of reversible redox reactions coupled with bulk ion insertions under conditions of AbrSV has been published [5]. The aim of this work is to extend our previous study of the kinetics of irreversible surface reactions [6, 7].

Because of its particulate nature, the microcrystalline solid is consumed to a significant extent during the measurement, and hence no steady-state dissolution currents can be obtained as is possible using compact disk electrodes made of the solid being studied. As a result, the course of AbrSV electrochemical reactions is controlled not only by a potential dependence of the rate coefficients, but additionally by the progress of the initial attack on the solid and by the granulometric characteristics of the particles. The situation resembles that in thermogravimetry (TG) of microcrystalline solids. During decades of TG development, numerous approaches have been tested to describe heterogeneous reactions of particle populations, and the resulting knowledge would also seem to be beneficial for AbrSV reaction kinetics.

T. Grygar (✉)
Institute of Inorganic Chemistry, Academy of Sciences,
250 68 Řež, Czech Republic

One of the basic principles of TG is the assumption that two contributions to the reactivity of microcrystalline solids may be separated: the influence of reaction temperature and that of the extent of a solid particle consumption (conversion), y [8]

$$\frac{dy}{dt} = k(T) f(y)$$

The goal of this separation is to obtain the activation energy, E_A, from the equation $k(T) = A \exp(-E_A/RT)$, whereas $f(y)$ includes all properties corresponding to a particle size and shape and to the geometry of a reaction course. A similar approach could be proposed for electrochemistry to obtain a function characterising the influence of potential:

$$\frac{dy}{dt} = k(E) f(y) \tag{1}$$

where $\frac{dy}{dt} = \frac{I}{Q_0}$ is a reduced reaction rate, Q_0 is the total charge of the electrochemical process, $k(E)$ is a potential-dependent rate coefficient, $y = 1 - \frac{Q(t)}{Q_0}$ is a reaction conversion, and $Q(t)$ is the charge corresponding to the rest of an electrochemical process from conversion $y = y(t)$ to $y = 1$. In fact, all previous attempts to describe the kinetics of electrochemical reactions of solid particles [9, 10, 11, 6] have been based on a similar separation of potential- and conversion-dependent functions, but only the simplest cases have so far been modelled and studied. Utilisation of Eq. 1 is meaningful only if charge transfer is the rate-determining step or if the charge transfer is significant in the overall reaction.

Several serious problems could occur as a result of the separation of $f(y)$ and $k(T)$. The most important problems met with in TG are: the processing non-isothermal reaction curves is much less reliable than that of isothermal ones [12], kinetic characteristics may change at different reaction temperatures [13], nucleation kinetics requires a certain incubation (induction) time, which shifts the time scale, and nucleation and growth kinetics may be differently affected by changing temperature [14]. As a result, the independence of $k(T)$ on y as well as $f(y)$ on temperature may be questioned in a particular case. Similar problems could be expected in AbrSV also.

The functions $k(E)$ obtained by studying compact metal-oxide electrodes can be adopted for AbrSV. The reaction course is not complicated by geometric factors ($f(y)$ in Eq. 1), so that $k(E)$ is directly and reliably obtained, but the applicability of this experimental method is naturally limited to sufficiently conducting metal oxides. Two such examples have already been sufficiently minutely described: the oxidative dissolution of UO_2 [15, 16] and the reductive dissolution of Fe_3O_4 [17–20]. Both these oxides are almost metallic conductors [21]. In both cases, the electrochemical reaction can be considered an irreversible process following Butler-Volmer kinetics (Eq. 2):

$$k(E) = k_{eq} \exp\left(-\frac{\alpha n F}{RT}(E - E_{eq})\right) = k_0 \exp(-aE) \tag{2}$$

Equation 2 was also applied for oxidative dissolution of metal particles from carbon paste electrodes (CPE) [9], reduction of copper oxide [10], and dissolution of iron oxides in CPE [11] as well as by AbrSV [6]. In the case of UO_2, the growth of $k(E)$ with growing over-potential is limited by the final rate of product removal from the electrode surface [15, 16]. Equation 2 is valid at least in the range between the potential that allows us to neglect a back reaction and the potential at which the reaction rate becomes saturated because of limitations imposed by the rest of the reaction steps. Unfortunately, there are many possible limits of the former kind: subsequent reactions of a primary product of the electrode reaction (oxidation of Cr^{III}), detachment of ions from the surface of crystals, dissolution of a possible secondary solid phase (U oxides), and diffusion of soluble ions to the bulk of the solution.

In contrast to the oxidation of UO_2, the function $k(E)$ possesses a peaked shape in the case of Fe_3O_4 reduction over a wider potential range [17–20], and this is related to the Engell [22] and Vermilyea [23] relationship (Eq. 3) (see also [4, 10, 24] for a review)

$$\frac{dy}{dt} = \frac{2\left(\frac{dy}{dt}\right)_{fr}}{\exp(a_+(E - E_{fr})) + \exp(-a_-(E - E_{fr}))} \tag{3}$$

In Eq. 3, according to Vermilyea, a_+ and a_- characterise cationic and anionic components, and the subscript fr corresponds to a freely dissolved crystal (without external applied potential). A "chemical" meaning of Eq. 3 is somewhat unclear, because its derivation is based on the separation of anion and cation removal from the oxide surface through the Helmholtz layer. Vermilyea supposed, that E_{fr} is equal to the potential of a zero surface charge during the dissolution, i.e., to the potential at which the surface of the dissolved crystal is of the same stoichiometry as its bulk. At $E \neq E_{fr}$, the surface composition of crystals changes with respect to this bulk stoichiometry, and either anions or cations prevail on the dissolved surface. Vermilyea concluded that the dissolution at $E \neq E_{fr}$ is slower at overpotentials of both signs. Because the rest potential of Fe_3O_4 is far more positive than the potential of the maximum dissolution rate (see the results of White et al. [19]), the anodic and cathodic branches of the function $k(E)$ were proposed to be determined by $\{O^{2-}\}$ and $\{Fe^{2+}\}$ removal, respectively [19], with the corresponding formal charge transfer coefficients a_+ and a_- according to the Vermilyea equation (Eq. 3). The objections to the application of Eq. 3 to ferric oxides can be briefly summarised as follows [10]: separated fluxes of O^{2-} and Fe^{2+} do not leave the dissolved surface, but the complex, hydrated species $[Fe(H_2O)_x(OH)_{6-x}]^{2-x}$ does. In any case, ion transfer through the diffusion double layer is supposed to control the dissolution of Fe_3O_4 in acids [24].

The second term on the right hand side of Eq. 1, $f(y)$, may be chosen from a wide variety of models offered by TG studies (see Fig. 1, and [8, 13]). The models should describe a possible development of particle geometry
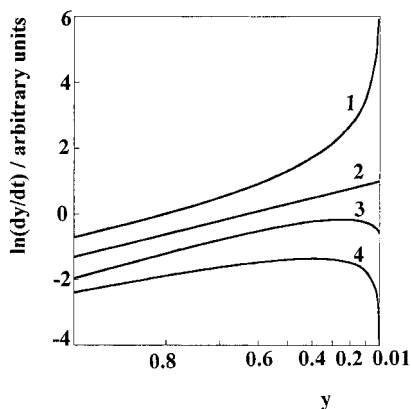
Fig. 1 The most frequently used functions $f(y)$ in a double logarithmic scale $\ln(\mathrm{d}y/\mathrm{d}t)$ vs $\ln(1-y)$. Reaction conversion is given on the x-axis for clarity. *1* Jander equation (diffusion through a layer of solid reaction product), *2* a general reaction order (a surface chemical reaction), *3* modified Šesták-Berggren equation, *4* Avrami-Erofeev nucleation kinetics. Kinetic equations from [8, 13] (curves 1, 2, 4) and Eq. 6 (curve 3)

and reactivity during the reaction, i.e., formation of reactive interfaces (nucleation), growth and overlap of the nuclei, changes of reactive surface area due to the particle consumption, and finally an influence of formation of secondary phases on the reactive surface. The importance of choosing the right $f(y)$ follows from the requirement for its virtual independence on E (or T in TG). Many particular $f(y)$ functions can be related to a known kinetic law [8, 13], and hence a reaction mechanism can be postulated, such as surface reaction, diffusion control, nucleation kinetics etc. However, when the formal kinetics is too complicated and a corresponding geometrical model could not be supported by independent experimental methods, even empirical $f(y)$ functions are utilised to fit experimental data and particularly to obtain E_A.

From the variety of the models, particularly the shrinking sphere model or a more general case frequently denoted as general reaction order kinetics, have been most frequently used [4, 6, 9, 11] for the case of an immediate reaction on the whole reactive surface of the solid:

$$f(y) = (1-y)^{\gamma} \tag{4}$$

Equation 4 yields monotonously decreasing curves of $\mathrm{d}y/\mathrm{d}t$ vs time (curve 2 in Fig. 1). Equation 4 is exactly valid only for a shape-preserving surface reaction of monodisperse particles, and is approximately valid for a general surface reaction of polydisperse crystals. The term γ is a complex function of a particle shape and a size distribution.

Whenever the initial reaction rate increases up to its local maximum at $0 < y < 1$ (curve 4 in Fig. 1), the Avrami-Erofeev equation [25, 26] is commonly used

$$1 - y = \exp\left(-(kt)^{\beta}\right)$$

This equation is used in TG [8, 13, 14] but also in dissolution kinetics [4]. Instead of it, a simpler power function also known from TG [13]

$$y \propto t^{n}$$

has been reported for the nucleation at the start of the electrochemical reduction of oxide films formed anodically on Co [27]. Neither of these two latter equations seems to be suitable for electrochemical modelling because the initial reaction rate at $y = 0$ is zero, and this would complicate the modelling of the linear sweep voltammetric curves. The same is also true for the empirical Šesták-Berggren equation (Eq. 5) [8, 14], which is formally a flexible alternative to the Avrami-Erofeev kinetics

$$\frac{\mathrm{d}y}{\mathrm{d}t} \propto y^{\delta}(1-y)^{\gamma} \tag{5}$$

However, Eq. 5 may be linearly combined with the shrinking particle model according to Eq. 4 [28], yielding

$$\frac{\mathrm{d}y}{\mathrm{d}t} \propto \left(k_{\mathrm{ini}} + (1-k_{\mathrm{ini}})y^{\delta}\right)(1-y)^{\gamma} \tag{6}$$

which avoids the zero initial rate. For $k_{\mathrm{ini}} = 1$, Eq. 6 changes to Eq. 4 and for $k_{\mathrm{ini}} = 0$ to Eq. 5, and hence it is also formally applicable to Avrami-Erofeev kinetics [8, 14]. The meaning of γ is the same as in Eq. 4, and δ is given by the geometry of the formation of new reactive surfaces. We are aware of the empirical nature of Eq. 6, but it is flexible enough to simulate various shapes of $f(y)$, and we show below the influence of $f(y)$ on AbrSV curves. Moreover, a non-zero initial reaction rate, growing with increasing conversion in the early stages, was observed in the course of electrochemical dissolution of α-FeOOH [29], and a similar course is common also in the case of α-Fe$_2$O$_3$ (Grygar, unpublished results). No suitable function $f(y)$ for such kinetics has yet been reported.

The third frequently occurring form of the $f(y)$ function should also be mentioned here, i.e. that in which the reaction rate is almost constant up to a certain stage, when it starts to decrease sharply. This case is sometimes denoted as "thin-layer" kinetics. The following may account for this behaviour: (a) an electroactive component is rapidly dissolved before the electrode reaction, and hence its concentration is close to the saturated value up to the solid phase consumption [30], (b) the electrode reactions are limited by the interfacial area between a thin layer of solution containing the electroactive species [31–33], or (c) an electroactive compound is deposited in a thin layer on the working electrode [31, 32]. These cases have been discussed in ferrocene oxidation and V_2O_5 reduction [30–33]). Dissolution of metal oxides is rarely controlled by diffusion [4], but very similar behaviour is formally obtained for dissolution of very thin plates via a surface reaction [28]. This case is rarely referred to in TG, but it seems to be important in dissolution kinetics.

Diffusion through a layer of a solid product frequently controls thermal decomposition of solids. Fast deceleration of an initial reaction rate is typical for this case (curve 1 in Fig. 1 [8]). This reaction course is not typical for dissolution reactions where soluble products are expected.

It is worth mentioning here that there is also a way to avoid the necessity to know the right $f(y)$ in thermal analysis, called a "time-to" method, which is only based on the independence of $f(y)$ on actual temperature [34]. Generally speaking, any kinetic equation $f(y)$, including empirical ones, may be used for studying $k(T)$ or $k(E)$ whenever they fit experimental data, and these are virtually independent on the intensive variables (T and E, respectively).

Equations 2 and 4 were used to derive the following relationships for the relative peak height and peak potential of linear sweep voltammetric curves of metal particles [9] and Fe and Cr oxides [6]:

$$\frac{I_P}{Q_0} = av\gamma^{\frac{\gamma}{1-\gamma}}$$

$$E_P = -\frac{1}{a}\ln(av) + \frac{1}{a}\ln(k_0)$$

where $a = \alpha nF/RT$, v is a scan rate, γ is the kinetic characteristic of Eq. 4, k_0 is the reaction rate coefficient at the reference potential. However, certain deviations have been observed using these equations. Because Eq. 2 is valid only over a limited potential interval, the peak currents I_P are lower than calculated ones [6]. This deviation is now reconsidered with particular respect to the above-described complexity of the kinetic behaviour of the particulate reactant, and the AbrSV reaction kinetics is discussed in a more general sense. Attention has also been paid to our assumption that a complete electrochemical dissolution of poorly conducting α-FeOOH, α-Fe$_2$O$_3$, γ-Fe$_2$O$_3$, ferrites, and α-Cr$_2$O$_3$ proceeds under conditions of AbrSV [6, 7, 35].

Experimental

α-Cr$_2$O$_3$ was prepared by thermal decomposition of ammonium dichromate and by subsequently heating the residue at 500 °C for 2 h. It is composed of rounded crystals with specific surface area $\sigma = 24\,m^2\,g^{-1}$. CrO$_2$ was obtained by hydrothermal synthesis from CrO$_3$ in an autoclave [36]. It is composed of elongated crystals with $\sigma = 18\,m^2\,g^{-1}$. γ-Fe$_2$O$_3$ was obtained from Fe$_3$O$_4$ by heating at 250 °C for 2 h [37], and hence it retained its cubic crystal shape ($\sigma = 4.5\,m^2\,g^{-1}$). α-Fe$_2O_3$ was prepared by evaporating solution of a ferric salt with citric acid, drying and burning the residue, and heating the product at 800 °C. The resulting α-Fe$_2$O$_3$ is composed of particles in the micron size range with well-defined edges according to transmission electron micrographs. The phase purity of all investigated solids was checked by XRD diffraction. The specific surface areas were obtained by a chromatographic method involving sorption of an N$_2$/H$_2$ mixture (for γ-Fe$_2$O$_3$) or by BET (for the other samples).

AbrSV was performed as described in [6, 7, 35]. The working electrode surface was cleaned by dry silica and filter paper. As a supporting electrolyte, 2 M H$_2$SO$_4$ was used for chromium oxides, and 0.1 M HClO$_4$ and 0.4 M NaClO$_4$ for iron oxides. All potentials are related to a reference saturated calomel electrode ($+0.241$ V vs standard hydrogen electrode).

Kinetic behaviour was modelled using a popular spreadsheet (Supecalc5). Modelling was used as a general tool to avoid the necessity for finding exact solutions of kinetic equations, certain of which would require numeric methods.

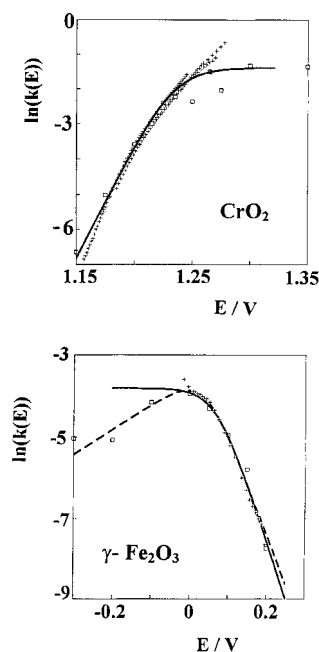## Processing electrochemical dissolution data

The summary of $f(y)$ used for the potentiostatic dissolution curve fitting is given in Table 1. Changes of the exponential constants of $f(y)$ with potential were observed in all studied cases. In line with previous findings, the γ parameter in Eq. 4 increases with increasing $k(E)$. In the case of Cr oxides, it is limited to 1.6 (CrO$_2$) and ~ 2.5 (α-Cr$_2$O$_3$). The parabolic function $y = kt - bt^2$ of γ-Fe$_2$O$_3$ corresponds to the model of thin polydisperse plates [28]. It may alternatively be fitted by the modified Šesták-Berggren equation (Eq. 6). The reason of such behaviour is unclear because the particles are of a cubic shape. The most probable explanation for the sigmoidal dissolution curves of α-Fe$_2$O$_3$ is the preferential propagation of the reaction along crystal dislocations and/or edges [38].

The changes of $f(y)$ with changing potential is in contradiction to what was stated in the Introduction about the required independence of $f(y)$ on the intensive variable E. As a result, only the initial values of the rate coefficient $k(y=0)$ can be used to search for $k(E)$, and the voltammetric curves can be used only up to their systematic deviation from chronoamperometric experiments. It would be necessary to know the actual reaction mechanism to explain these deviations; however, the limitations caused by the reactions following the charge transfer would in general be suspected, such as saturation by Fe^{2+} or CrO$_4^{2-}$ of the solution surrounding the dissolved crystals. In any case, an initial reaction rate may be supposed to be free of these "secondary" limits. Nevertheless, the changes of the γ (and δ) parameters do not limit the formal applicability of Eqs. 4 and 6. The corresponding reaction rate coefficients were further used as the best possible estimates of $k(E)$.

Table 1 $f(y)$ utilised for fitting potentiostatic dissolution curves

Solid phase	$f(y)$	Limits of $f(y)$ validity
α-Cr$_2$O$_3$, CrO$_2$	General reaction order Eq. 4	$k(E) < k_{MAX}$
γ-Fe$_2$O$_3$, α-Fe$_2$O$_3$	modified Šesták-Berggren Eq. 6	The entire potential range
γ-Fe$_2$O$_3$	$y = kt - bt^2$, "thin plate" model [28]	The entire potential range
CrO$_2$	"	$k(E) \to k_{MAX}$

Fig. 2 The dependence of the reaction rate coefficient on potential, $k(E)$, for CrO_2 oxidative dissolution and for γ-Fe_2O_3 reductive dissolution. $k(E)$ values were obtained by potentiostatic ($\square$) and potentiodynamic ($+$) experiments. The *solid lines* represent fits according to SCM (Eq. 8), and the *dashed line* that according to Engell and Vermilyea (Eq. 3)

chemical redox dissolution of Fe and Cr oxides can be adopted [4, 39, 40]. Its rate is driven by the detachment of metal ions from the surface metal sites with changed valence and with relatively fixed coordination surroundings. This approach is suitable for the redox dissolution of semiconducting and covalent oxides. According to this surface complexation model (SCM), the final rate of metal oxide dissolution is reached when the solid-particle surface is saturated by the reactive surface sites. For example, during reductive dissolution of iron(III) oxides, "soluble" surface sites $\{\equiv Fe^{II}\}$ are formed by reduction of protonated $\{\equiv Fe^{III}\}$ sites [4, 39]. The validity of Eq. 2 for iron oxide electrochemical dissolution at low overpotential [6, 7, 29] implies that the formation of these reactive sites is controlled by the charge transfer reaction

$$\{\equiv Fe^{III}\} + e^- \xrightarrow{\ H^+\ } \{\equiv Fe^{II}\} \tag{7}$$
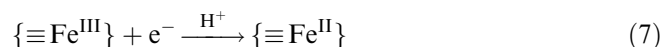
with the rate $\frac{d\{\equiv Fe^{II}\}}{dt} \propto k_{eq}\{\equiv Fe^{III}\}\exp(-aE_0)$. This reaction step is followed by a detachment of Fe^{2+} from the reactant surface and its diffusion to the solution. With respect to a final total amount of possible surface sites, we obtain

$$k(E) = \frac{k\exp(-aE)}{1 + k\exp(-aE)}k_{MAX} \tag{8}$$

where k_{MAX} corresponds to the surface completely covered by $\{\equiv Fe^{II}\}$ (for more details see Appendix A). The oxidative dissolution of α-Cr_2O_3 can have a similar reaction mechanism, but it is based on $\{\equiv Cr^{IV}\}$ and/or $\{\equiv Cr^V\}$ surface intermediates formed by oxidation of $\{\equiv Cr^{III}\}$ [4, 40]. Equation 8 was successfully used to fit the experimental data (see Fig. 2 and Table 2).

The maximal reaction rate coefficient k_{MAX} is determined by the rate of detachment of $\{\equiv Fe^{II}\}$ from completely reduced surface of Fe oxide, either by a chemical reaction

$$\{\equiv Fe^{II}\} \xrightarrow{\ H^+\ } Fe^{2+}(aq) \tag{9}$$

or by a simple diffusion of Fe^{2+}. In both these cases, k_{MAX} is not a function of potential.

Diffusion is the fastest possible mechanism for completing the dissolution after the charge transfer step,

$$J_{dif} = \frac{D}{\delta}c_{sat}S_1$$

where D is diffusivity, δ is a thickness of a diffusion layer, c_{sat} is the saturated concentration of Fe^{2+} in supporting electrolyte, and S_1 is a surface area of a single

Examples of the functions $k(E)$ obtained by oxidation of CrO_2 and reduction of γ-Fe_2O_3 are given in Fig. 2. Potentiostatic measurements are represented directly by the rate coefficients. Potentiodynamic curves of chromic oxides presented in Fig. 2 obtained at 1, 2, 5, and $10\,mV\,s^{-1}$ were transformed according to the equation

$$k(E) = \ln(I/Q_0) - \gamma\ln(Q/Q_0)$$

A corresponding relationship based on Eq. 6 was used for γ-Fe_2O_3 potentiodynamic data processing ($1\,mV\,s^{-1}$). In both cases shown in Fig. 2, Butler-Volmer kinetics (Eq. 2) is valid only in a relatively narrow potential range. The $k(E)$ of γ-Fe_2O_3 may be described by the Engell-Vermilyea relationship (Eq. 3), but it is not valid for chromium oxides studied. The $k(E)$ functions of α-Fe_2O_3 and α-Cr_2O_3 are of the same type as that of CrO_2, i.e., the rate is saturated at a sufficiently high overpotential, giving a roughly constant value denoted by k_{MAX}. The characteristics of $k(E)$ so obtained are summarised in Table 2.

Modelling electrode kinetics

To obtain an appropriate $k(E)$ for *electrochemical* dissolution of the metal oxides, the reaction mechanism of

Table 2 The parameters of $k(E)$ obtained for studied iron and chromium oxides. In the case of α-Fe_2O_3, k_{ini} according to Eq. 5 and only potentiostatic curves were processed

Solid phase	$k(E)$	a	Rate coefficients
α-Cr_2O_3	Eq. 8	40	$k_0 = 3 \cdot 10^{-25}\,s^{-1}, k_{MAX} = 0.03\,s^{-1}$
CrO_2	Eq. 8	65	$k_0 = 4 \cdot 10^{-36}\,s^{-1}, k_{MAX} = 0.25\,s^{-1}$
α-Fe_2O_3	Eq. 8	21	$k_0 = 1.2 \cdot 10^{-4}\,s^{-1}, k_{MAX} = 0.0013\,s^{-1}$
γ-Fe_2O_3	Eq. 8	29	$k_0 = 0.17\,s^{-1}, k_{MAX} = 0.022\,s^{-1}$
	Eq. 3	$a_+ = 6, a_- = 25$	$k_{fr} = 0.017\,s^{-1}(E_{fr} = 0.04\,V)$

particle. Because of the definition of the rate coefficient by Eq. 1, this equation can be re-written for an initial reaction rate

$$\frac{(J_{\text{dif}})_{y=0}}{N_0} = \frac{D}{\delta} c_{\text{sat}} \sigma M_R = k_{\text{dif}}$$

where σ is a specific surface area and M_R is the weight of solid giving 1 mol of the reaction product. For $D \approx 10^{-5}\,\text{cm}^2\,\text{s}^{-1}$, $c_{\text{sat}} \approx 10\,\text{mol}\,\text{dm}^{-3}$, $\sigma \approx 20\,\text{m}^2\,\text{g}^{-1}$, and $M_R \approx 80\,\text{g}\,\text{mol}^{-1}$, k_{dif} is roughly in the order of $10^{-8}/\delta_{y=0}\,\text{s}^{-1}$. Note that the k_{MAX} decreases in the order $CrO_2 > Cr_2O_3 > \gamma\text{-}Fe_2O_3 > \alpha\text{-}Fe_2O_3$, and the specific surface areas $CrO_2 \approx Cr_2O_3 > \gamma\text{-}Fe_2O_3 > \alpha\text{-}Fe_2O_3$. A possible chemical reaction leading to detachment of Fe^{2+} will be slower than diffusion. However, both these are surface processes, and hence the general validity of Eq. 4 is to be expected. Naturally, change of reaction mechanism to diffusion control will affect the value of γ.

If Eq. 9 is interpreted as the transfer of cations from negatively charged surface through the diffusion double-layer against a potential gradient $\Delta\psi$, Eq. 8 may be transformed into

$$k(E) = \frac{k\exp(-aE)}{1 + k\exp(-aE)} k_{\text{MAX},\Delta\psi=0} \exp(zF\Delta\psi/RT) \quad (10)$$

where z is the charge of an evolved ion. However, this "electrostatic" interpretation is rather exceptionally correct, because the ΔG for ion transfer $(10–30\,\text{kJ}\,\text{mol}^{-1})$ is usually much smaller than the overall ΔG for metal oxide dissolution (frequently $> 70\,\text{kJ}\,\text{mol}^{-1}$) [4]; the case of Fe_3O_4 described in the Introduction looks to be rather an exception. Note that if $\Delta\psi$ were a linear function of the electrode potential, Eq. 10 could easily be formally rearranged to Eq. 3, which is formally valid for Fe_3O_4 electrochemical dissolution (see the Introduction). Unfortunately, the relationship between E and $\Delta\psi$ is probably more complex [24]. Having regard to all the mentioned facts and hypotheses mentioned above and irrespective of the particular formalism of Eqs. 3 and 10, the only explanation of the peak-shaped $k(E)$ is the rather unusual mechanism of the product removal from a reacting surface via diffusion through the electrified diffusion layer. The nature of Eq. 10 seems to be more realistic than that of Eq. 3, and additionally it is compatible with Eq. 8. The coefficient a of Eq. 3 could simply mean a diffusion of H^+ required for dissolution to the surface more positive

Fig. 3 The influence of the decreasing k_{MAX} in SCM (Eqs. 8 and 4) on voltammetric curves obtained at $1\,\text{mV}\,\text{s}^{-1}$. Kinetic characteristics: $a = 20\,\text{V}^{-1}$, $\gamma = 1.2$, $k_0 = 1\,\text{s}^{-1}$, and with $k_{\text{MAX}} \to \infty$ (curve 1), $k_{\text{MAX}} = 0.1\,\text{s}^{-1}$ (curve 2), $0.03\,\text{s}^{-1}$ (curve 3), $0.01\,\text{s}^{-1}$ (curve 4), and $0.003\,\text{s}^{-1}$ (curve 5)
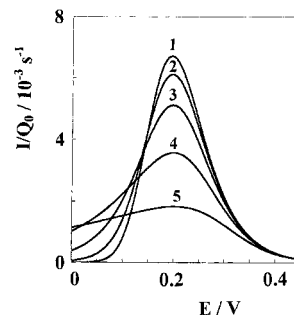
than E_{fr} $(E > E_{\text{fr}})$ and a_+ for transport of $[Fe(H_2O)_x(OH)_{6-x}]^{2-x}$ from the surface at $E < E_{\text{fr}}$.

The $k(E)$ for $\gamma\text{-}Fe_2O_3$ dissolution (Fig. 2) can hence be qualitatively explained as an "intermediate" between Eqs. 2 and 3 with $a_+ \ll a_-$ (Table 2), i.e., as the surface-complexation process with a little contribution from electrostatic effects in the saturated region of $k(E)$. In the case of magnetite, a_+ and a_- are of similar size [17–20].

Voltammetric curves as a function of $k(E)$ and $f(y)$

Modelling shows that saturation of the reaction rate according to Eq. 8 leads to the decrease of the peak current I_P/Q_0 and the increase of Q_P/Q_0 with respect to the original relationships based on Butler-Volmer kinetics [6, 9] that distort voltammetric peaks in a manner shown in Fig. 3. The influence of the $k(E)$ saturation is particularly important at greater scan rates (Table 3). At the same time, the peak potential shifts slightly anodically. The experimental observations of the peak current and peak symmetry [6, 7] are in line with these tendencies. For the studied microcrystalline metal oxides, scan rates less than $0.1\,\text{mV}\,\text{s}^{-1}$ should be used to avoid these effects [7].

Regardless of the particular mathematical form of $k(E)$ (Eq. 3 or 10), its local maximum causes the voltammetric peak potential not to be controlled mainly by the solid phase consumption, as it is in the case of all other models mentioned in this work. The peak shifts with changing reaction rate less than in the case of other $k(E)$ values used here, and, after faster scans, subsequent scans can reveal that a part of the solid remains unaltered, although the current drops almost to zero even in the first scan.

Table 3 Modelled linear sweep voltammetric curves for general reaction order $f(y)$ with $\gamma = 1.2$ and combined with Eq. 2 or Eq. 4 with $\alpha = 0.25$ and $k_{\text{MAX}} = k_0 = 0.01\,\text{s}^{-1}$, $E_{\text{eq}} = 0\,\text{V}$

$k(E)$	Simple exponential Eq. 2			Surface complexation model, Eq. 8		
v, $\text{mV}\,\text{s}^{-1}$	y_P	$I_P/(v \cdot Q_0)$, $10^3\,\text{s}^{-1}$	E_P, V	y_P	$I_P/(v \cdot Q_0)$, $10^3\,\text{s}^{-1}$	E_P, V
0.1	0.60	3.35	0.230	0.58	3.19	0.231
0.2	0.60	3.35	0.161	0.56	3.05	0.163
0.5	0.60	3.35	0.069	0.52	2.71	0.073
1	0.60	3.35	0.000	0.46	2.30	0.006
2	0.60	3.35	−0.069	0.39	1.79	−0.061
5	0.60	3.35	−0.161	0.28	1.10	−0.149

Table 4 Modelled peak characteristics obtained by combining Eq. 2 and Eq. 6. $\gamma = 1.2$, $\delta = 0.8$, $\alpha = 0.5$, and $k_0 = 0.01\ \text{s}^{-1}$, $E_{eq} = 0\ \text{V}$

k_{ini}	y_P	$I_P/(v \cdot Q_0)$, $10^3\ \text{s}^{-1}$	E_P, V
1	0.60	6.69	−0.035
0.9	0.60	6.87	−0.038
0.6	0.60	7.59	−0.049
0.3	0.61	9.04	−0.064
0.1	0.58	11.6	−0.079
0.03	0.56	14.4	−0.090
0.01	0.55	16.6	−0.097

When the modified Šesták-Berggren equation (Eq. 6) is used as $f(y)$, the voltammetric peaks are higher and shift cathodically with decreasing k_{ini} (Table 4 and Fig. 4) and increasing δ. In other words, the more pronounced the initial growth of $f(y)$, the more negative and higher are the voltammetric peaks that arise. If the resulting sharp peak were fitted erroneously according to Eqs. 2 and 4, bigger α values would be obtained (Fig. 4). Only a potentiostatic measurement may undoubtedly reveal the real shape of $f(y)$. This situation resembles that of TG: the same final shape of the TG curve may be obtained with different sets of $f(y)$ and E_A. A corresponding example is demonstrated in Fig. 4, where solid and dashed lines 2 represent almost identical voltammetric peaks but obtained by a quite different a and $f(y)$.

Conclusions

A reliable evaluation of the kinetics of irreversible reactions of microcrystalline electroactive solids requires the separation of the two main contributions to the reactivity of the solids: a potential-dependent rate coefficient $k(E)$ and a conversion-dependent function $f(y)$. Although their mathematical separation for potentio-dynamic data fitting seems to be formally easy, it is
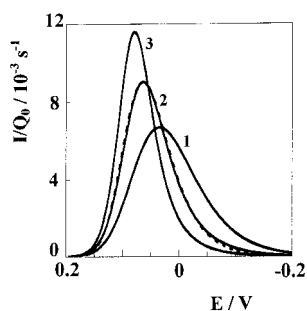

Fig. 4 The influence of k_{ini} on the voltammetric peaks according to Eqs. 2 and 6. Scan rate $1\ \text{mV s}^{-1}$, kinetic characteristics $\gamma = 1.2$, $\delta = 0.8$, $a = 20\ \text{V}^{-1}$, $k_0 = 0.01\ \text{s}^{-1}$, $k_{ini} = 1$ (curve 1), 0.3 (curve 2), and 0.1 (curve 3). The curve with $k_{ini} = 1$ corresponds in fact to the non-sigmoidal $f(y)$ according to Eq. 4. *Dashed line* represents the system with $\gamma = 1.2$, $k_0 = 0.0048\ \text{s}^{-1}$ and $a = 27\ \text{V}^{-1}$

preferable to perform the potentiostatic dissolution at different potentials to obtain independent estimates of both $k(E)$ and $f(y)$. Both $k(E)$ and dy/dt can be monotonous functions as well as functions with a local maximum, and they both affect peak potentials and peak currents in AbrSV of a microcrystalline solid. As a result, peak potentials alone or their dependence on the scan rate cannot be used for the characterisation of the electrode kinetics as it is common in the voltammetry of soluble species (see the summary in Table 5).

To describe the kinetics of irreversible electrode reactions of microparticles, the following procedure can be recommended:

1. Obtaining $f(y)$ from potentiostatic experiments (a complete dissolution of the studied solid) and the comparison of $f(y)$ to the models described in this work or in the thermoanalytical literature (see also Fig.1)
2. Obtaining $k(E)$ from potentiostatic experiments performed at various potentials
3. Only if the kinetic model $f(y)$ does not alter significantly in the potential range, where the corresponding voltammetric peak occurs, $k(E)$ can be obtained also from potentiodynamic experiments, and E_P can be discussed safely.

The validity of a general reaction order (Eq. 4) with the γ around unity may indicate a simple surface reaction [6], whereas sigmoidal reaction curves (e.g., Eq. 6) indicate anisotropic crystals (α-FeOOH [29], α-Fe$_2$O$_3$) and/or new-phase nucleation kinetics.

The properties of $k(E)$ bring additional information about the course of the reaction. "Saturated" $k(E)$ (α-Cr$_2$O$_3$, CrO$_2$, α-Fe$_2$O$_3$) can be attributed to the surface-complexation mechanism [4, 39] with product removal either by subsequent surface chemical reaction or by simple diffusion. As follows from the theoretical considerations (see Introduction), the peak-shaped $k(E)$ (Fe$_3$O$_4$) requires a further theoretical explanation, but this type of $k(E)$ indicates that the removal of the reaction product is controlled by ion transfer through a diffusion double layer. Intermediate behaviour (γ-Fe$_2$O$_3$) indicates a less significant influence of the ion transfer along with the prevailing chemical nature of Fe^{2+} detachment. In both cases, a formal charge transfer coefficient can be obtained.

A very similar formal kinetics of oxidative dissolution of CrO$_2$ (metallic conductor) and α-Cr$_2$O$_3$ (semiconductor) shows that AbrSV is not limited to the study of metal oxides with a high electronic conductivity. The proposed explanation is based on the conducting reacting surface formed via protonation and introduction of electron-hopping centres. It creates an opportunity to collect and compare data of dissolution reactions of metal oxides of different conductivity.

Table 5 A summary of characteristics determining the shape of a voltammetric peak of an irreversible reaction of a microcrystalline solid reactant

$k(E)$	$f(y)$	E_P determined by	I_P/Q_0 determined by	Examples	Reference
$k_0\exp(-aE)$	$(1-y)^\gamma$	k_0, α	α, γ, v	All studied oxides at low overpotentials	[6, 15–19, 22, 23, 35, 7]
$\dfrac{k_0\exp(-aE)}{1 + k_0/k_{MAX}\exp(-aE)}$	$(1-y)^\gamma$	k_0, α	$k_{MAX}, \alpha, \gamma, \sim v^{0.5}$	α-Fe$_2$O$_3$, α-Cr$_2$O$_3$, CrO$_2$	This study
$k_0\exp(-aE)$	$\left(k_{ini} + (1-k_{ini})y^\delta\right)(1-y)^\gamma$	$k_0, k_{ini}, \alpha, \delta$	$k_{MAX}, \alpha, \gamma, \delta, v$	α-Fe$_2$O$_3$	This study
$\dfrac{k_{fr}}{\exp\left(a_+(E-E_{fr})\right) + \exp\left(-a_-(E-E_{fr})\right)}$	$(1-y)^\gamma$	$E_{fr}, \alpha_+, \alpha_-\gamma$	$k_{fr}, \alpha_+, \alpha_-, \gamma, v$	Fe$_3$O$_4$, γ-Fe$_2$O$_3$	[17–19, 22, 23]

Appendix A: Surface complexation of electrochemically dissolved metal oxides

In strongly acidic solution, the surface sites $\{\equiv Fe^{III}\}$ are fully protonated. The resulting complex may be dissolved either by further attack by protons, ligands, and/or by an action of reducing ions such as ascorbate, ferrous oxalate, and sulfide [4, 39]. The reduction pathway is much faster than the proton-promoted one. The overall rate of the ferric oxide dissolution is hence controlled predominantly by the amount of $\{\equiv Fe^{II}\}$ according to Eq. 9:

$$\{\equiv Fe^{II}\} \xrightarrow{H^+} Fe^{2+}(aq)$$
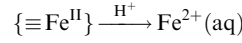
$$J_{dis} \approx k_{dis}\{\equiv Fe^{II}\}$$

The $\{\equiv Fe^{II}\}$ intermediates are formed by a charge transfer reaction (Eq. 7). At low overpotential, the overall rate of electrochemical reductive dissolution is controlled by Butler-Volmer kinetics (Eq. 2), and hence this charge transfer is an irreversible reaction and the rate-determining step. Assuming that the dissolving solid surface is sufficiently conducting, the rate of the formation of new $\{\equiv Fe^{II}\}$ is

$$J_{CT} = k_{CT}\{\equiv Fe^{III}\}\exp(-aE) \tag{11}$$

Because the sum of $\{\equiv Fe^{III}\}$ and $\{\equiv Fe^{II}\}$ is equal to a constant, $\{\equiv Fe_{TOT}\}$, and because $J_{dis} = J_{CT}$ during the steady state dissolution, we obtain by a simple rearrangement

$$J_{dis} = \frac{k_{CT}k_{dis}\exp(-aE)}{k_{dis} + k_{CT}\exp(-aE)}\{\equiv Fe_{TOT}\}$$

The saturated J_{dis} is reached when $k_{CT}\exp(-aE) \gg k_{dis}$ and hence when the surface is completely covered by $\{\equiv Fe^{II}\}$. Let us denote the corresponding saturated reaction rate coefficient by $k_{MAX} = k_{dis}\{\equiv Fe_{TOT}\}$. Hence

$$J_{dis} = \frac{k_{CT}/k_{dis}\exp(-aE)}{1 + k_{dis}/k_{CT}\exp(-aE)}k_{MAX}$$

and, to employ a denotation compatible with Eq. 2,

$$J_{dis} = \frac{k_0\exp(-aE)}{1 + k_0/k_{MAX}\exp(-aE)}$$

The latter equations are identical to Eq. 8.

The applicability of this approach is limited to the case when the charge-transfer propagation of the redox process is sufficiently fast. Electron hopping between $\{\equiv Fe^{II}\}$ and $\{\equiv Fe^{III}\}$ can theoretically mediate reaction spreading over the entire surface. This electron hopping between surface sites with a similar crystal structure is sufficiently fast, but it requires the presence of comparable fractions of both electron-hopping centres [21]. On the contrary, if the electron hopping was the rate-determining step, a gradient of $\{\equiv Fe^{II}\}$ would be formed and the reaction could be hardly treated as a surface reaction controlled, as was claimed in [7]. A possible consequence of this gradient is demonstrated in Appendix B and Fig. 5B and treated in [5].

Note that this mixed-valence region on the surface of dissolving metal oxide particles should substantially increase the surface electric conductivity regardless of its bulk properties. The thickness of this mixed-valence region is limited by the depth of proton diffusion which is necessary for the reduction of $\{\equiv Fe^{III}\}$, or by OH$^-$ or H$_2$O diffusion for $\{\equiv Cr^{III}\}$ oxidation. The propagation of the reaction over the entire solid particle surface is then enabled by electron hopping between adjacent surface sites with different metal ion valences. This electron hopping within a uniform crystal lattice is fast enough [21] to make the charge transfer reaction (Eq. 7) quasi-reversible. The existence of such a surface conducting layer may explain the complete dissolution of pure and substituted α-FeOOH under conditions of AbrSV [7].

It is worth mentioning here that the H$^+$ diffusion to the surface layers of reductively dissolved ferric oxides was also assumed by
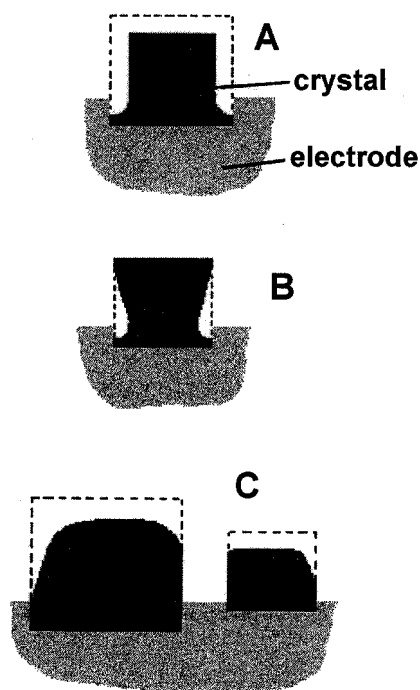
Fig. 5A–C A simplified geometry of electrochemical attack of the microcrystals deposited on the working electrode surface according to the nature of the rate-determining step: **A** surface reaction, **B** electron hopping under insufficient bulk conductivity, **C** diffusion removal of the resulting Fe^{2+}. For details see Appendix B

Figure 5C shows a possible geometry of the diffusion-limited dissolution when the surroundings of crystals are saturated by Fe^{2+}. The most exposed edges are dissolved the fastest. The method of sample deposition could play a key role in such a process. Only the course of the reaction in its initial stage could be compared with that of the surface reaction (Fig. 5A), because in the latter stages the particle shape and hence also the sense of the function $f(y)$ will change, and the dissolution rate will decrease because of increase of the diffusion layer δ. This kind of attack is most probable at potentials of the saturated reaction rate according to Eq. 8 if k_{MAX} is controlled by the diffusivity of the metal ions. The validity of the "thin-plate" model (CrO_2 at the most positive potentials, see Table 1) is in accordance with the course depicted in Fig. 5C.

References

1. Scholz F, Lange B (1992) Trends Anal Chem 11: 359
2. Scholz F, Meyer B (1994) Chem Soc Rev 341
3. Brainina KhZ, Neyman E (1993) Electroanalytical stripping methods. Wiley, New York
4. Blesa MA, Morando PJ, Regazzoni AE (1994) Chemical dissolution of metal oxides. CRC, Boca Raton, Fla
5. Lovrić M, Scholz F (1997) J Solid State Electrochem 1: 108
6. Grygar T (1996) J Electroanal Chem 405: 117
7. Grygar T (1997) J Solid State Electrochem 1: 77
8. Šesták J (1984) Thermophysical properties of solids, their measurements and theoretical analysis. Elsevier, Amsterdam
9. Brainina KhZ, Vydrevich MB (1981) J Electroanal Chem 121: 1
10. Goritschev IG, Kipriyanov NA (1981) Zh Fiz Khim 55: 2734 (in Russian)
11. Mouhandess MT, Chassagneux F, Vittori O, Accary A, Reeves RM (1984) J Electroanal Chem 181: 93
12. Criado JM, Ortega A, Real C, Torres de Torres E (1984) Clay Miner 19: 653
13. Dollimore D, Tong P, Alexander KS (1996) Thermochim Acta 282/283: 13
14. Cumbrera FL, Sánchez-Bajo F (1995) Thermochim Acta 266: 315
15. Nicol MJ, Needs CRS (1975) Electrochim Acta 20: 585
16. Nicol MJ, Needs CRS (1977) Electrochim Acta 22: 1381
17. Haruyama S, Masamura K (1978) Corros Sci 18: 263
18. Mancey DS, Shoesmith DW, Lipkowski J, McBride AC, Noël J (1993) J Electrochem Soc 140: 637
19. White AF, Peterson ML, Hochella Jr MF (1994) Geochim Cosmochim Acta 58: 1859
20. Allen PD, Hampson NA, Bignold GJ (1980) J Electroanal Chem 111: 223
21. Cox PA (1995) Transition metal oxides, an introduction to their electronic structure and properties, 2nd edn. Clarendon, Oxford
22. Engell HJ (1956) Z Phys Chem 7: 158
23. Vermilyea DA (1966) J Electrochem Soc 113: 1067
24. Bruyere VIE, Blesa M (1985) J Electroanal Chem 182: 141
25. Avrami M (1939) J Chem Phys 7: 1103; (1940) 8: 212; (1941) 9: 177
26. Erofeev BV, Comptes Rendus URSS (1946) 52: 511
27. Gervasi CA, Biaggio SR, Vilche JR, Arvia JR (1991) Electrochim Acta 36: 2147
28. Grygar T, Ruan HD, ACH Models in Chemistry (in print)
29. Grygar T, Šubrt J, Boháček J (1995) Coll Czech Chem Commun 60: 950
30. Lamache M, Bauer D (1977) J Electroanal Chem 79: 359
31. Laviron B (1978) J Electroanal Chem 90: 33
32. Gavasso R, Laviron B (1979) J Electroanal Chem 102: 249
33. Ramírez MT, Palomar ME, González I, Rojas-Hernández A (1995) Electroanalysis 7: 184
34. Goss CJ (1987) Miner Mag 51: 437
35. Grygar T (1996) Coll Czech Chem Commun 61: 93

Goritschev and Kipriyanov [10] on the base of experimental data (an isotope exchange between solution and dissolved solid and the hysteresis of dissolution currents at changing potential).

Appendix B: Rate-determining step and geometry of dissolution

The complete sequence of the redox dissolution of metal oxides includes many steps that could possibly become the rate determining step.

Figure 5A–C demonstrates how the nature of the rate-determining step controls the geometry of the electrochemical dissolution of microcrystals. All the models used here for modelling the course of dissolution are based on the assumption of a free reaction of all crystal faces exposed to the solution (Fig. 5A). This reaction course resembles a surface chemical reaction of suspended solids if we neglect the depth of particle immersion into the working electrode surface. This reaction course is limited to the case when the surface reaction (Eq. 9) is the rate-determining step, i.e. when the solubility limit of Fe^{2+} has not yet been reached around the crystal.

If the conductivity of dissolved solid was low and the electron hopping could not allow free spreading of the reactive centres over the solid-solution interface, a gradient of the surface-site concentration would arise. Such a case would lead to the geometry represented in Fig. 5B. In such a case, the interpretation of the experimentally obtained kinetic characteristics should be substantially different from the one presented above. As already pointed out [7], the preferential or even exclusive dissolution of the crystal parts in the ternary interface solid-electrode-solution according Fig. 5B should have decreased the value of γ with respect to a free surface reaction because of decrease of the dimensionality of the crystal attack; this was not observed.

36. Swoboda TJ, Arthur P, Cox NL, Ingraham JN, Oppegard AL, Sadler MS, J Appl Phys (1961) 32: 374S
37. Schwertmann U, Cornell RM (1991) Iron oxides in the laboratory. VCH, Weinheim
38. Cornell RM, Giovanoli R (1993) Clay Miner 28: 223
39. Zinder B, Furrer G, Stumm W (1986) Geochim Cosmochim Acta 50: 1861
40. Segal MG, Williams WJ (1986) J Chem Soc, Faraday Trans 82: 3245